Article:
Niwase, T., Watanabe, Y. X., Hirayama, Y. et al. (17 more authors) (2023) Discovery of New Isotope 241U and Systematic High-Precision Atomic Mass Measurements of Neutron-Rich Pa-Pu Nuclei Produced via Multinucleon Transfer Reactions. Physical Review Letters. 132502. ISSN: 1079-7114

https://doi.org/10.1103/PhysRevLett.130.132502

Editors' Suggestion | Featured in Physics

Discovery of New Isotope ^{241}U and Systematic High-Precision Atomic Mass Measurements of Neutron-Rich Pa-Pu Nuclei Produced via Multinucleon Transfer Reactions

T. Niwase,[1,*] Y. X. Watanabe,[1] Y. Hirayama,[1] M. Mukai,[2] P. Schury,[1] A. N. Andreyev,[3] T. Hashimoto,[4] S. Iimura,[5] H. Ishiyama,[2] Y. Ito,[6] S. C. Jeong,[1] D. Kaji,[2] S. Kimura,[2] H. Miyatake,[1] K. Morimoto,[2] J.-Y. Moon,[4] M. Oyaizu,[1] M. Rosenbusch,[1] A. Taniguchi,[7] and M. Wada[1]

[1]*Wako Nuclear Science Center, Institute of Particle and Nuclear Studies, High Energy Accelerator Research Organization (KEK), Wako, Saitama 351-0198, Japan*
[2]*RIKEN Nishina Center for Accelerator-Based Science, Wako, Saitama 351-0198, Japan*
[3]*School of Physics, Engineering and Technology, University of York, York YO10 5DD, United Kingdom*
[4]*Institute for Basic Science, 70, Yuseong-daero 1689-gil, Yusung-gu, Daejeon 43000, Korea*
[5]*Department of Physics, Rikkyo University, Tokyo 171-8501, Japan*
[6]*Advanced Science Research Center, Japan Atomic Energy Agency, Ibaraki 319-1195, Japan*
[7]*Institute for Integrated Radiation and Nuclear Science, Kyoto University, Kumatori, Osaka 590-0494, Japan*

(Received 21 November 2022; revised 26 January 2023; accepted 16 February 2023; published 31 March 2023)

The new isotope ^{241}U was synthesized and systematic atomic mass measurements of nineteen neutron-rich Pa-Pu isotopes were performed in the multinucleon transfer reactions of the $^{238}\mathrm{U} + {}^{198}\mathrm{Pt}$ system at the KISS facility. The present experimental results demonstrate the crucial role of the multinucleon transfer reactions for accessing unexplored neutron-rich actinide isotopes toward the $N = 152$ shell gap in this region of nuclides.

DOI: 10.1103/PhysRevLett.130.132502

Of the presently known nuclides, ∼300 are naturally occurring while another ∼3000 have been artificially produced, the heaviest being $^{294}_{118}$Og (oganesson) [1]. Furthermore, according to modern theoretical calculations, more than 4000 further radioactive nuclei are expected to exist [2–4], mostly in the region of the neutron-rich isotopes, which are believed to be produced in the astrophysical r process [5]. A strong worldwide push across several existing and planned facilities is underway to expand the chart of nuclides, toward both the proton and neutron drip lines, with particular emphasis on the heaviest elements [6,7]. The discovery of new nuclides at the edges of stability often critically challenges the existing nuclear models, helping to refine them [3,7,8].

The stability or existence of an isotope depends on its binding energy, which in the simplest approximation, can be expressed as the sum of a bulk macroscopic part (the "liquid-drop contribution") and a microscopic shell correction energy. In most nuclides, especially in the light region, the former contribution is dominant, but the shell corrections can play a substantial role and often result in dramatic nuclear structure changes, as documented in many cases across the chart of nuclei [9,10].

On the contrary, in the region of high atomic number ($Z \gtrsim 100$), the strong Coulomb repulsion between protons makes the macroscopic contribution relatively small such that it alone cannot bind superheavy nuclides (SHN) [3,11]. Because of this, the mere existence of SHN is defined by a shell correction energy which is manifested in the creation of nucleonic subshell closures of spherical or deformed nature, enhancing the stability of a nucleus [12,13]. For example, in the actinide and transactinide regions, the deformed subshell closures at $Z = 108$ and $N = 162$, and $Z = 100 - 102$ and $N = 152$ have long been predicted [14–17]. Figure 1 shows a plot of the ground state shell correction energy as calculated by a macroscopic-microscopic model (FRDM12 [18]) for the $_{90}$Th-$_{102}$No nuclides around $N = 152$. An island of strong shell corrections with values as low as about −5 MeV is centered around $_{100}$Fm-$_{102}$No. Indeed, evidence of the deformed shell closure at $N = 152$ was first established as early as the 1950s [19,20] and its nature has since been experimentally confirmed by various methods, e.g., through observation of rotational bands and high-spin K isomers [21,22], and measurements of masses [23] and spontaneous fission half-lives [24]. A primary reason for the richness of experimental data in this area is its accessibility via fusion reactions between partners close to doubly magic $^{208}_{82}$Pb and $^{48}_{20}$Ca, which result in enhanced production cross sections [25].

However, the shell effect is predicted to be strongly suppressed to values around −1 MeV, for the neutron-rich $_{90}$Th-$_{94}$Pu nuclides with $N = 152$, see Fig. 1. At present, only scarce experimental data exist for this region [26,27], because of the difficulty to reach it experimentally, which is clearly demonstrated by the closeness of the line of known

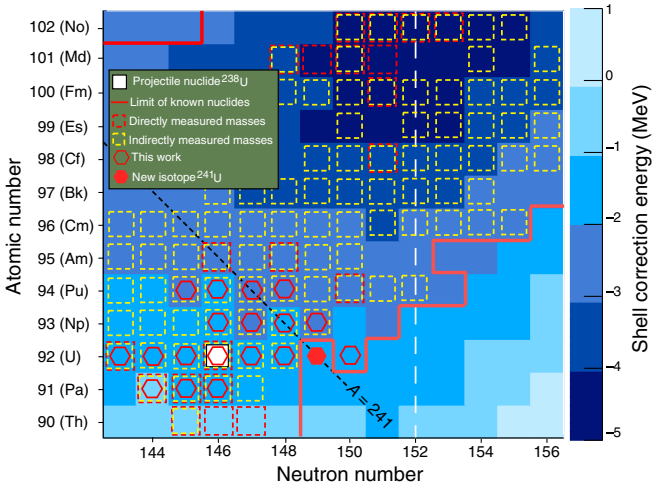

FIG. 1. Microscopic shell correction energy calculated with the FRDM12 [18] for the region spanning $Z = 90 - 102$ and $N = 143 - 156$. The red lines indicate the limits of known isotopes. For nuclides with known mass, the methods of determination—direct and/or indirect—are noted. The hexagons denote the isotopes whose masses were directly measured in this work.

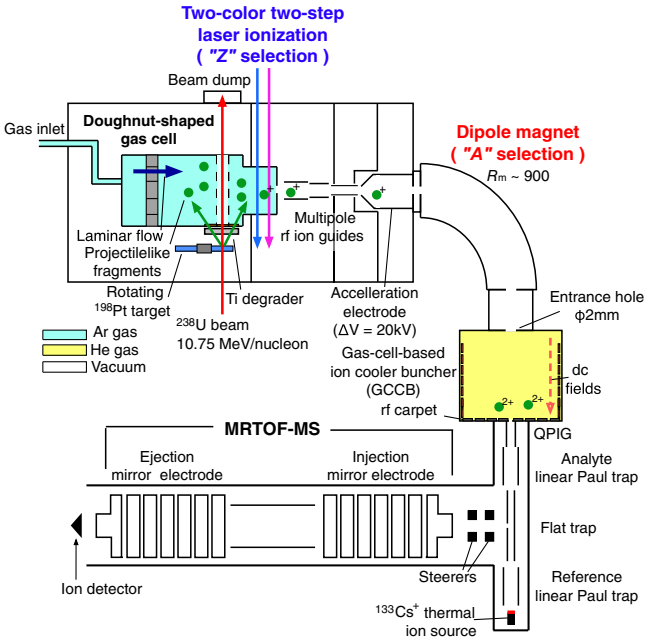

FIG. 2. Sketch of the KISS experimental setup. The blue- and yellow-colored areas are filled with Ar and He gases, respectively. Differential pumping systems are located after the doughnut-shaped gas cell as well as before and after the GCCB.

isotopes to the β-stable $^{238}_{92}$U nuclide. However, the decay properties, such as half-lives, decay modes, and in particular fission of the neutron-rich actinide and transactinide nuclei may play a crucial role in elucidating the still unrevealed pathway of r-process nucleosynthesis beyond the $N = 126$ shell closure [5,28]. Investigating the behavior of the $N = 152$ shell gap in the lower-Z elements from $_{91}$Pa to $_{94}$Pu is an important issue for understanding of the shell evolution in the neutron-rich actinide region. Furthermore, the properties of nuclei in the vicinity of the deformed gap at $N = 152$ may provide a microscopic benchmark for nuclear models for superheavy nuclides with $Z > 114$ [21,22].

Multinucleon transfer (MNT) reactions, in which nucleons flow in both directions between the target and the projectile nuclei, are expected to be a powerful technique for synthesis and study of nuclides in the neutron-rich actinide region [29]. Recently, they have begun to be used in laboratories around the world, such as JAEA [30], GANIL [31], and GSI [32]. In addition, there are several new MNT-based facilities in planning or under construction: the $N = 126$ factory at ANL [33], NEXT at Groningen [34], and INCREASE at GSI [35].

The KEK Isotope Separation System (KISS) is a recently-commissioned facility for the nuclear spectroscopy of nuclides produced via MNT reactions, installed at the RIKEN Nishina Center [36,37]. KISS has successfully extracted neutron-rich isotopes of the refractory elements Pt, Ir, and Os, which were produced as targetlike fragments using the $^{136}_{54}\mathrm{Xe} + ^{198}_{78}\mathrm{Pt}$ reaction system [38–41]. By stopping MNT products in a flowing gas, KISS has demonstrated an advantage for studying the neutron-rich isotopes of these elements, which are difficult to extract from traditional ISOL targets. In addition, a multireflection time-of-flight mass spectrograph (MRTOF MS), which was installed recently, provides high-precision mass measurements [42]. In this Letter, we report on the first systematic mass measurements of neutron-rich Pa-Pu isotopes produced as projectilelike fragments (PLF) via several MNT channels of the $^{238}_{92}\mathrm{U} + ^{198}_{78}\mathrm{Pt}$ reaction at the KISS facility, resulting in the high-precision direct determination of the masses of 19 nuclides and the discovery of a new uranium isotope $^{241}_{92}$U.

An overview of the KISS experimental setup is shown in Fig. 2. A primary beam of $^{238}_{92}$U [10.75 MeV/nucleon, typical intensity of ~30 particle nA (1 particle nA is 6.2×10^9 particles/s)], accelerated by the RIKEN Ring Cyclotron, impinged for four days upon a rotating $^{198}_{78}$Pt (enriched to 91.63%) target [37] with a thickness of 12.5 mg/cm^2. The isotopes of interest were produced as PLFs in the MNT reactions, having masses and velocities close to those of the primary beam particles, and being scattered around the grazing angle. The energy of these reaction products was attenuated by a 40-μm Ti energy degrader to maximize the fraction stopping in a doughnut-shaped gas cell [37] filled with 65-kPa argon gas.

The PLFs were neutralized in the gas cell, and transported to the gas-cell exit, where they were ionized by a two-color two-step resonant laser ionization technique. A dye laser pumped by an excimer laser (XeCl,

$\lambda = 308$ nm, Lambda Physik, LPX240i) was used for the first step excitation with a tunable wavelength, λ_1, which corresponds to the energy of an excited state specific to the element. For each of the eleven nuclides of primary interest —$^{235-237}_{91}$Pa, $^{238-242}_{92}$U, and $^{239-241}_{93}$Np—an appropriate value of λ_1 was used. Where not known previously, the values for λ_1 were extrapolated from well-known resonance wavelengths or measured resonance wavelengths with more abundantly produced isotopes, considering their isotope shifts [43]. Another excimer laser of the same model was used for the ionization step with the fixed wavelength of $\lambda_2 = 308$ nm, which was suitable for the ionization of all elements of our interest following the first excitation step. The extracted singly charged ions were transported by a set of multipole radio-frequency (rf) ion guides through a differentially pumped region and accelerated to 20 keV [37]. The accelerated ions were mass separated according to their mass-to-charge ratios by a dipole magnet with a mass-resolving power of $R_m \sim 900$. Those ions, selected in both atomic and mass number, passed through a differentially pumped region and stopped in the windowless gas-cell-based ion cooler buncher (GCCB) [42] filled with 120-Pa He gas for ion trapping prior to performing high-precision mass measurements. Most ions were extracted from the GCCB as doubly charged ions, having lost an electron in their collisions with the He gas atoms [44]. An electric dc field was used to guide the stopped ions to an rf carpet [45] that further guided the ions to a small extraction orifice. After being extracted from the GCCB, they were transported by a quadrupole rf ion guide (QPIG) followed by a linear Paul trap to be accumulated in the "flat trap" [46]. After being cooled by the dilute helium buffer gas (< 0.1 Pa), finally the ions were injected into the MRTOF MS.

In order to determine the absolute mass values from the measured time-of-flight (TOF) as well as to correct the drift of the TOF, $^{133}_{55}$Cs$^+$ reference ions, from a thermal ion source installed on the side of the flat trap opposite to the GCCB (see Fig. 2) were detected concomitantly with the analyte ions [47]. Figure 3(a) shows a typical TOF spectrum of the reference ion after 1000 laps, resulting in a mass resolving power of $R_m \approx 260\,000$. The representative TOF value was determined by fitting the TOF spectral peak with an empirical Gaussian hybrid function [41].

The atomic mass m of an ion with charge q was obtained using the single-reference method from the mass m_r and the charge q_r of the reference ion [48,49],

$$m = \frac{q}{q_r}\rho^2(m_r - q_r m_e) + q m_e, \qquad \rho = \left(\frac{t_m - t_0}{t_r - t_0}\right), \quad (1)$$

where m_e is the electron mass, ρ is the TOF ratio between the analyte and reference ions, while t_m and t_r are the measured TOF for the analyte and reference ions, respectively. The flat trap ejection delay t_0 was determined from a

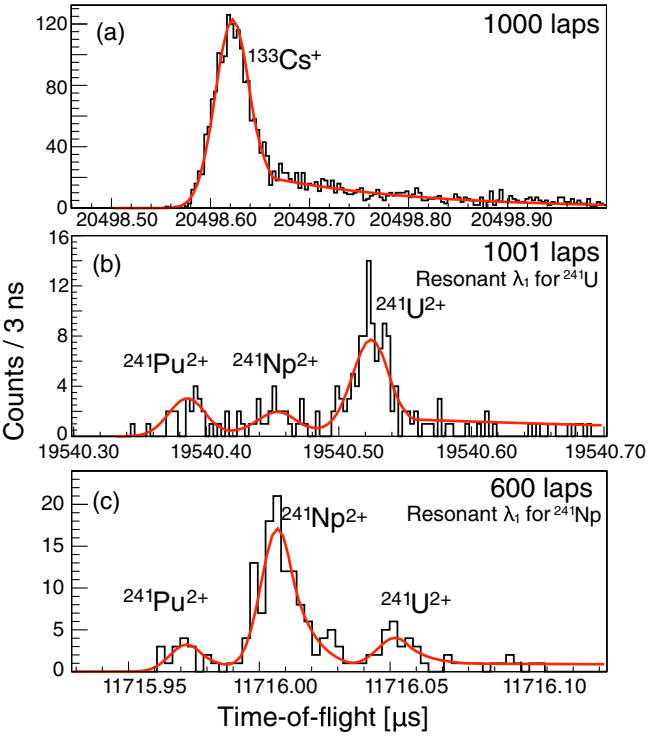

FIG. 3. Typical TOF spectra with the red solid lines denote the fitting curves. (a) The reference ion $^{133}_{55}$Cs$^+$ after 1000 laps in the MRTOF MS. (b) $A/q = 120.5$ region after 1001 laps in the MRTOF MS with $\lambda_1 = 387.217$ nm for the new isotope $^{241}_{92}$U. (c) $A/q = 120.5$ region after 600 laps with $\lambda_1 = 385.062$ nm for $^{241}_{93}$Np. The absolute TOF values between (b) and (c) are different due to the difference in the number of laps.

measurement of ρ^2 for the well-known ions $^{238}_{92}$U^{2+} and $^{133}_{55}$Cs$^+$.

Figure 3(b) shows the TOF spectrum at 1001 laps with resonant wavelength for the new isotope $^{241}_{92}$U. As seen in the TOF spectrum, nonresonantly ionized isobars of higher-yield nuclides were delivered alongside the resonantly ionized species of interest, allowing for a wide-ranging systematic mass measurement campaign. Figure 3(c) shows the TOF spectrum at 600 laps with resonant wavelength for $^{241}_{93}$Np. The comparison of the spectra in Figs. 3(b) and 3(c) evinces the identification of the new isotope $^{241}_{92}$U.

We have successfully measured the masses of 19 actinide isotopes from $A = 235$ to 242, including the eight non-resonantly ionized nuclides $^{235-237}_{92}$U, $^{242}_{93}$Np, and $^{239-242}_{94}$Pu. The resulting mass excesses, ME_{EXP}, and respective laser wavelengths λ_1 are listed in Table I, and the differences between our experimental data and the data listed in AME2020 [50], Δm, are shown in Fig. 4. The uncertainties of the mass values were defined as a standard deviation of the χ^2 fitting. This is the first direct mass measurements for most of the nuclides (see Fig. 1). All measured masses agree with the AME2020 values within the uncertainties. The previously unknown masses of $^{241,242}_{92}$U, which had

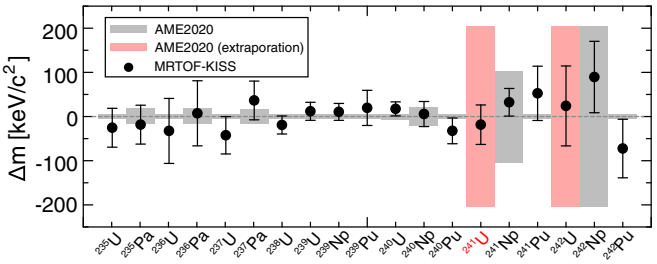

FIG. 4. Difference of the present masses from those listed in AME2020. The gray shadows show the experimental AME2020 uncertainties, while the red color indicates the extrapolated ones for $^{241,242}_{92}$U.

been evaluated with an uncertainty of 200 keV/c^2 in AME2020 by extrapolation based on the trend of measured masses of neighboring nuclides, have been determined experimentally for the first time as $ME(^{241}_{92}\mathrm{U}) = 56\,182(45)$ keV/c^2 and $ME(^{242}_{92}\mathrm{U}) = 58\,644(90)$ keV/c^2. The counting rates of $^{241,242}_{92}$U were 6.2×10^{-3}, and 2.0×10^{-3} counts per second, respectively. The masses of $^{241,242}_{93}$Np had been only measured indirectly from the end points of their β-ray energies with large uncertainties of 100 and 200 keV/c^2, respectively [50]. They were successfully measured directly in this experiment as $ME(^{241}_{93}\mathrm{Np}) = 54\,352(31)$ keV/c^2, and $ME(^{242}_{93}\mathrm{Np}) = 57\,509(81)$ keV/c^2, with significantly improved uncertainties.

In order to assess the $N = 152$ shell gap for U and Np isotopes, we use a two-neutron shell gap parameter Δ_{2n} [51] defined as

$$\Delta_{2n}(N,Z) = m(N-2,Z) + m(N+2,Z) - 2m(N,Z), \tag{2}$$

where $m(N,Z)$ is the mass of nuclide having Z protons and N neutrons. A nucleus with a closed (sub)shell has a relatively high binding energy among neighboring nuclei, resulting in an enhanced Δ_{2n} value. Figure 5 shows Δ_{2n} plots of $_{102}$No, $_{93}$Np, and $_{92}$U, where the extrapolated AME2020 mass values were used for $^{248-251}_{102}$No, $^{243-245}_{93}$Np, and $^{243}_{92}$U, because their masses are not experimentally known. The experimental Δ_{2n} data of No isotopes clearly show a peak at $N = 152$ [23,52], indicating the existence of the shell gap at $Z = 102$. The comparison of Δ_{2n} between the measurements and theoretical mass models provides a critical test for calculations toward the extreme regions of the nuclear chart. The prediction by five theoretical models, a shell model (DZ10 [53]), macroscopic-microscopic model (FRDM12 [18] and WS4$^{\mathrm{RBF}}$ [54]), a microscopic self-consistent mean-field model (HFB32 [55]), and phenomenological mass model (KTUY05 [2]) are shown with different colored lines. The trend of the No isotopes is reproduced by FRDM12 and WS4$^{\mathrm{RBF}}$. The trends of the U and Np isotopes are well described for $N < 150$ in all

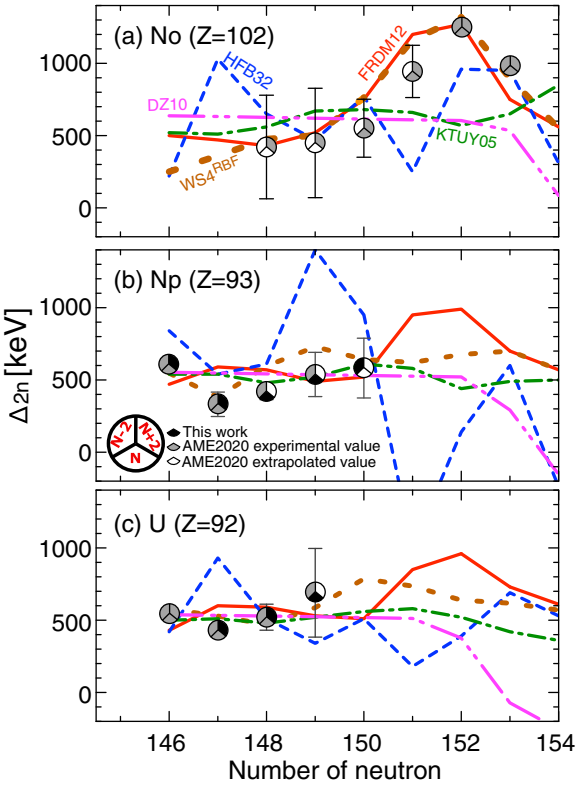

FIG. 5. Two-neutron shell gap parameter Δ_{2n} for (a) $_{102}$No, (b) $_{93}$Np, and (c) $_{92}$U isotopes. Data points are divided into three segments to indicate which mass data are used for three masses contributing to $\Delta_{2n}(N,Z)$ [upper left: $m(N-2,Z)$, upper right: $m(N+2,Z)$, and bottom: $m(N,Z)$]. Black segment indicates experimental values from this work. White and gray segments show the extrapolated and experimental values from AME2020, respectively. The extrapolated masses have typical uncertainty of $\delta m \sim 200$ keV/c^2. Solid and dashed lines represent the calculations from the various theoretical mass models specified in the top panel, DZ10 [53], FRDM12 [18], WS4RBF [54], HFB32 [55], and KTUY05 [2].

model calculations except for HFB32. However, in the region of unknown isotopes above $N = 150$, there are variations of up to ~1000 keV among them, with only FRDM12 exhibiting peaks at $N = 152$. Therefore, in order to probe the existence of this subshell closure at the lighter actinide elements, the discovery and studies of further neutron-rich actinide nuclides are mandatory. This work demonstrated that we can readily push beyond the pioneering foray by the TRIGA-TRAP [56] toward the $N = 152$ region of lower-Z nuclides using MNT reactions.

To conclude, Table I summarizes the results of first systematic mass measurements of northeast of $^{238}_{92}$U by a combination of the isotope separator KISS and a high-precision mass spectrograph MRTOF MS. The first identification of $^{241}_{92}$U, produced by an MNT reaction in the $^{238}_{92}\mathrm{U} + ^{198}_{78}\mathrm{Pt}$ system, was made by mass spectrometry. This establishes a new method to investigate this scarcely studied and hard to reach region. These results demonstrate

TABLE I. The first excitation step laser wavelength λ_1, the square of the measured time-of-flight ratio: ρ^2 between analyte ions and the reference ion $^{133}_{55}Cs^+$, and mass excesses from the measurements (ME_{EXP}). No λ_1 values are listed for nonresonantly ionized isotopes.

Nuclide	λ_1 (nm)	ρ^2	ME_{EXP} (keV/c^2)
^{235}U	⋯	0.884 252 029(207)	40 893(44)
^{235}Pa	387.452	0.884 257 591(207)	42 270(44)
^{236}U	⋯	0.888 020 252(341)	42 412(74)
^{236}Pa	387.456	0.888 032 082(342)	45 341(74)
^{237}U	⋯	0.891 794 198(195)	45 348(42)
^{237}Pa	387.456	0.891 803 150(203)	47 564(44)
^{238}U	387.213	0.895 564 126(94)	47 289(20)
^{239}U	387.214	0.899 339 527(93)	50 585(20)
^{239}Np	385.056	0.899 334 426(88)	49 322(19)
^{239}Pu	⋯	0.899 331 542(182)	48 608(40)
^{240}U	387.216	0.903 110 293(72)	52 733(16)
^{240}Np	385.058	0.903 108 632(129)	52 322(28)
^{240}Pu	⋯	0.903 099 630(133)	50 093(29)
^{241}U	387.217	0.906 886 310(203)	56 182(45)
^{241}Np	385.062	0.906 878 922(142)	54 352(31)
^{241}Pu	⋯	0.906 873 491(279)	53 008(61)
^{242}U	387.218	0.910 658 345(409)	58 644(90)
^{242}Np	⋯	0.910 653 763(366)	57 509(81)
^{242}Pu	⋯	0.910 642 192(300)	54 644(66)

the strong feasibility of extending future studies to decay spectroscopy and even decay-correlated mass spectrometry [49,57] of neutron-rich actinides.

Furthermore, using a heavier-symmetric projectile and target combinations such as $^{238}_{92}U + ^{238}_{92}U$ or $^{248}_{96}Cm$ is promising for reaching more exotic nuclei toward the comprehensive understanding of the r process and to investigate the evolution of nuclear structure at $N = 152$ and beyond. Based on present KISS efficiencies [37] and production yields expected by GRAZING and GRAZING-F calculations [58–60], it should be possible to reach up to $N = 154$ for elements from $_{90}$Th to $_{94}$Pu within reasonable accelerator beam times, using the $^{238}_{92}U + ^{238}_{92}U$ reaction system.

We express our gratitude to the RIKEN Nishina Center for Accelerator-based Science and the Center for Nuclear Science at University of Tokyo for their support of online measurements. This work was financially supported by the Japan Society for the Promotion of Science KAKENHI (Grants No. 23244060, No. 24740180, No. 26247044, No. 15H02096, No. 17H01132, No. 17H06090, No. 18H03711, No. 20H00169, No. 21H04479, No. 21J00670, No. 22H0 4946), and by U.K. STFC.

*tniwase@post.kek.jp

[1] Yu. Ts. Oganessian and K. Utyonkov, Nucl. Phys. **A944**, 62 (2015).
[2] H. Koura, T. Tachibana, M. Uno, and M. Yamada, Prog. Theor. Phys. **113**, 305 (2005).
[3] W. Nazarewicz, Nat. Phys. **14**, 537 (2018).
[4] G. G. Adamian, N. V. Antonenko, A. Diaz-Torres, and S. Heinz, Eur. Phys. J. A **56**, 47 (2020).
[5] J. J. Cowan, C. Sneden, J. E. Lawler, A. Aprahamian, M. Wiescher, K. Langanke, G. Martínez-Pinedo, and F. K. Thielemann, Rev. Mod. Phys. **93**, 015002 (2021).
[6] Yu. Ts. Oganessian and K. Utyonkov, Rep. Prog. Phys. **78**, 036301 (2015).
[7] M. Thoennessen, *The Discovery of Isotopes: A Complete Compilation* (Springer, New York, 2016).
[8] O. B. Tarasov *et al.*, Phys. Rev. Lett. **121**, 022501 (2018).
[9] K. Heyde and J. L. Wood, Rev. Mod. Phys. **83**, 1467 (2011).
[10] T. Otsuka, A. Gade, O. Sorlin, T. Suzuki, and Y. Utsuno, Rev. Mod. Phys. **92**, 015002 (2020).
[11] Z. Patyk, A. Sobiczewski, P. Armbruster, and K.-H. Schmidt, Nucl. Phys. **A491**, 267 (1989).
[12] M. Bender, W. Nazarewicz, and P.-G. Reinhard, Phys. Lett. B **515**, 42 (2001).
[13] A. Sobiczewski and K. Pomorski, Prog. Part. Nucl. Phys. **58**, 292 (2007).
[14] S. G. Nilsson, C. F. Tsang, A. Sobiczewski, Z. Szymański, S. Wycech, C. Gustafson, I.-L. Lamm, P. Möller, and B. Nilsson, Nucl. Phys. **A131**, 1 (1969).
[15] C. E. Bemis Jr. and J. R. Nix, Comments Nucl. Part. Phys. **7**, 65 (1977).
[16] S. Ćwiok, V. V. Pashkevich, J. Dudek, and W. Nazarewicz, Nucl. Phys. **A410**, 254 (1983).
[17] J. L. Egido and L. M. Robledo, Phys. Rev. Lett. **85**, 1198 (2000).
[18] P. Möller, A. Sierk, T. Ichikawa, and H. Sagawa, At. Data Nucl. Data Tables **109**, 1 (2016).
[19] A. Ghiorso, S. G. Thompson, G. H. Higgins, B. G. Harvey, and G. T. Seaborg, Phys. Rev. **95**, 293 (1954).
[20] A. M. Friedman, J. E. Gindler, R. F. Barnes, R. Sjoblom, and P. R. Fields, Phys. Rev. **102**, 585 (1956).
[21] P. Reiter *et al.*, Phys. Rev. Lett. **82**, 509 (1999).
[22] R.-D. Herzberg *et al.*, Nature (London) **442**, 896 (2016).
[23] E. M. Ramirez *et al.*, Science **337**, 1 (2012).
[24] F. P. Heßberger, Eur. Phys. J. A **53**, 75 (2017).
[25] S. Hofmann, Radiochim. Acta **99**, 405 (2011).
[26] R. E. Brown, J. A. Cizewski, E. R. Flynn, and J. W. Sunier, Phys. Rev. C **20**, 1301 (1979).
[27] H. Makii, T. Ishii, M. Asai, K. Tsukada, A. Toyoshima, M. Matsuda, A. Makishima, J. Kaneko, H. Toume, S. Ichikawa, S. Shigematsu, T. Kohno, and M. Ogawa, Phys. Rev. C **76**, 061301(R) (2007).
[28] T. Kajino and G. J. Mathews, Rep. Prog. Phys. **80**, 084901 (2017).
[29] V. Zagrebaev and W. Greiner, Phys. Rev. Lett. **101**, 122701 (2008).
[30] K. Hirose *et al.*, Phys. Rev. Lett. **119**, 222501 (2017).

[31] C. Rodríguez-Tajes *et al.*, Phys. Rev. C **89**, 024614 (2014).
[32] H. M. Devaraja, S. Heinz, D. Ackermann, T. Göbel, F. P. Heßberger, S. Hofmann, J. Maurer, G. Münzenberg, A. G. Popeko, and A. V. Yeremin, Eur. Phys. J. A **56**, 224 (2020).
[33] G. Savard, M. Brodeur, J. A. Clark, R. A. Knaack, and A. A. Valverde, Nucl. Instrum. Methods Phys. Res., Sect. B **463**, 258 (2020).
[34] J. Even, X. Chen, A. Soylu, P. Fischer, A. Karpov, V. Saiko, J. Saren, M. Schlaich, T. Schlathölter, L. Schweikhard, J. Uusitalo, and F. Wienholtz, Atoms **10**, 59 (2022).
[35] A. Rotaru, D. Amanbayev, D. L. Balabanski, D. Benyamin, P. Constantin, T. Dickel, L. Gröf, I. Mardor, I. Miskun, D. Nichita, W. R. Plaß, C. Scheidenberger, A. Spataru, and A. State, Nucl. Instrum. Methods Phys. Res., Sect. B **512**, 83 (2022).
[36] Y. Hirayama, Y. X. Watanabe, N. Imai, H. Ishiyama, S. C. Jeong, H. Miyatake, M. Oyaizu, S. Kimura, M. Mukai, Y. H. Kim, T. Sonoda, M. Wada, M. Huyse, Yu. Kudryavtsev, and P. Van Duppen, Nucl. Instrum. Methods Phys. Res., Sect. B **353**, 4 (2015).
[37] Y. Hirayama, Y. X. Watanabe, M. Mukai, M. Oyaizu, M. Ahmed, H. Ishiyama, S. C. Jeong, Y. Kakiguchi, S. Kimura, J. Y. Moon, J. H. Park, P. Schury, M. Wada, and H. Miyatake, Nucl. Instrum. Methods Phys. Res., Sect. B **412**, 11 (2017).
[38] Y. Hirayama, M. Mukai, Y. X. Watanabe, M. Ahmed, S. C. Jeong, H. S. Jung, Y. Kakiguchi, S. Kanaya, S. Kimura, J. Y. Moon, T. Nakatsukasa, M. Oyaizu, J. H. Park, P. Schury, A. Taniguchi, M. Wada, K. Washiyama, H. Watanabe, and H. Miyatake, Phys. Rev. C **96**, 014307 (2017).
[39] Y. Hirayama, Y. X. Watanabe, M. Mukai, M. Ahmed, S. C. Jeong, Y. Kakiguchi, S. Kimura, M. Oyaizu, J. H. Park, P. Schury, M. Wada, H. Watanabe, and H. Miyatake, Phys. Rev. C **98**, 014321 (2018).
[40] M. Mukai *et al.*, Phys. Rev. C **102**, 054307 (2020).
[41] H. Choi, Y. Hirayama, S Choi, T. Hashimoto, S. C. Jeong, H. Miyatake, J. Y. Moon, M. Mukai, T. Niwase, M. Oyaizu, M. Rosenbusch, P. Schury, A. Taniguchi, Y. X. Watanabe, and M. Wada, Phys. Rev. C **102**, 034309 (2020).
[42] J. Y. Moon, S. C. Jeong, M. Wada, P. Schury, Y. X. Watanabe, Y. Hirayama, Y. Ito, M. Rosenbusch, S. Kimura, S. Ishizawa, T. Niwase, H. Wollnik, and H. Miyatake, RIKEN Accel. Prog. Rep. **52**, 138 (2018).
[43] R. Engleman, Jr. and B. A. Palmer, J. Opt. Soc. Am. **70**, 308 (1980).
[44] P. Schury *et al.*, Nucl. Instrum. Methods Phys. Res., Sect. B **407**, 160 (2017).
[45] M. Wada *et al.*, Nucl. Instrum. Methods Phys. Res., Sect. B **204**, 570 (2003).
[46] Y. Ito, P. Schury, M. Wada, S. Naimi, C. Smorra, T. Sonoda, H. Mita, A. Takamine, K. Okada, A. Ozawa, and H. Wollnik, Nucl. Instrum. Methods Phys. Res., Sect. B **317**, 544 (2013).
[47] P. Schury, Y. Ito, M. Rosenbusch, H. Miyatake, M. Wada, and H. Wollnik, Int. J. Mass Spectrom. **433**, 40 (2018).
[48] Y. Ito, P. Schury, M. Wada, S. Naimi, T. Sonoda, H. Mita, F. Arai, A. Takamine, K. Okada, A. Ozawa, and H. Wollnik, Phys. Rev. C **88**, 011306(R) (2013).
[49] T. Niwase *et al.*, Phys. Rev. C **104**, 044617 (2021).
[50] M. Wang, W. J. Huang, F. G. Kondev, G. Audi, and S. Naimi, Chin. Phys. C **45**, 030003 (2021).
[51] K. Rutz, M. Bender, T. Bürvenich, T. Schilling, P.-G. Reinhard, J. A. Maruhn, and W. Greiner, Phys. Rev. C **56**, 238 (1997).
[52] M. Block *et al.*, Nature (London) **463**, 785 (2010).
[53] J. Duflo and A. P. Zuker, Phys. Rev. C **52**, R23 (1995).
[54] N. Wang and M. Liu, Phys. Rev. C **84**, 051303(R) (2011).
[55] S. Goriely, N. Chamel, and J. M. Pearson, Phys. Rev. C **93**, 034337 (2016).
[56] M. Eibach, T. Beyer, K. Blaum, M. Block, Ch. E. Düllmann, K. Eberhardt, J. Grund, Sz. Nagy, H. Nitsche, W. Nörtershäuser, D. Renisch, K. P. Rykaczewski, F. Schneider, C. Smorra, J. Vieten, M. Wang, and K. Wendt, Phys. Rev. C **89**, 064318 (2014).
[57] P. Schury *et al.*, Phys. Rev. C **104**, L021304 (2021).
[58] A. Winther, Nucl. Phys. **A572**, 191 (1994).
[59] A. Winther, Nucl. Phys. **A594**, 203 (1995).
[60] R. Yanez and W. Loveland, Phys. Rev. C **91**, 044608 (2015).